Estimation of anthropogenic heat flux and its coupling analysis with urban building characteristics -- A case study of typical cities in the Yangtze River Delta, China

Chen Yu[a, b], Deyong Hu[a, b*], Shasha Wang[a], Shanshan Chen[c], Yichen Wang[a, b]

[a] College of Resource Environment and Tourism, Capital Normal University, Beijing 100048, China

[b] Laboratory Cultivation Base of Environment Process and Digital Simulation, Beijing 100048, China

[c] Institute of Remote Sensing and Geographic Information System, School of Earth and Space Science, Peking University, Beijing 100871, China

Abstract

The anthropogenic heat emitted into the atmosphere has increased significantly in urban areas with accumulated building and increased energy consumption. Carrying out anthropogenic heat flux (AHF) estimation and exploring the correlation between the AHF and building characteristics (density and height) helps reveal the urban climate's genetic mechanism. This study took Shanghai, Nanjing, and Hangzhou, the typical cities in the Yangtze River Delta region of China as case studies. The annual AHF of 2000, 2008, and 2016 based on the energy consumption inventory and multi-source remote sensing data was estimated. Besides, the monthly AHF by time dimension downscaling processing was obtained. The correlation between AHF and building characteristics was then analyzed by combining urban classification and building block data. The results showed that the AHF of typical cities increased significantly from 2000 to 2016, and the difference between the AHF of building area and the whole city was 12.69-20.36 $W \cdot m^{-2}$. Monthly AHF had a stratification phenomenon in different building characteristics. Moreover, building characteristics' impact on monthly AHF in the winter was more evident than that in the summer. The AHF of the building growth region was higher than that of the non-growth region, and the differences were more significant in the winter months (1.94-2.23 W·m^{-2}) than in summer months (0.59-0.94 W·m^{-2}). Building density on AHF was more significant than building height, and its contribution was higher than 80% on average in typical cities.

Keywords: Anthropogenic heat flux; Building characteristic; Energy consumption inventory method; Time dimension downscaling; Yangtze River Delta

1 Introduction

Human beings consume various forms of energy in life and production, including industry, commerce, transportation, and human metabolism (Sailor et al., 2015). The heat generated by this energy consumption and emitted into the atmosphere is called anthropogenic heat (AH). When AH is emitted into the atmosphere, the near-surface air temperature may rise by 1-3 °C (Gutiérrez et al., 2015). AH is an essential component of the urban thermal environment that cannot be ignored. Many studies have shown that its emissions will not only affect the urban ecological environment (Doan et al., 2019; Yuan et al., 2020) but also have an adverse effect on human health and economic development (Chen et al., 2016a).

Anthropogenic heat flux (AHF) is the amount of AH emitted per unit time and area. Previous studies attempted to estimate global AHF (Allen et al., 2011; Dong et al., 2017; Flanner, 2009). These studies generally use the energy consumption inventory method, obtaining various types of energy data to get the estimated results. Meanwhile, in recent years, AHF research on the urban scale has become more common, and relevant work has been carried out in Singapore (Quah and Roth, 2012), London (Iamarino et al., 2012), Sydney (Ma et al., 2017), Los Angeles (Zheng and Weng, 2018), and Beijing (Yang et al., 2018). Introducing more accurate models and parameters can effectively improve the reliability of AHF estimation (Park et al., 2016; Sun et al., 2018; Wang et al., 2019b).

Energy consumption in urban areas has further increased with natural landscapes transform into artificial landscapes. AHF accumulates in economically developed and densely populated urban areas and tends to affect local energy balance and environmental climate variability. The distribution and morphological characteristics of urban industrial, commercial, and residential building areas are the primary heat emission sources and are crucial for estimating AHF (Adelia et al., 2019). Wong et al. (2015) pointed out that AHF was positively correlated with building density and height through their study in Hong Kong. Ziaul and Pal (2018) found that high-rise, densely built areas emitted relatively high AHF, and there was a significant numerical gradient of AHF reduction from the urban center to the periphery. AH has prominent aggregation characteristics, and the building area's AHF contribution is substantial (Boehme et al., 2015). The appearance of buildings has changed the regional structure, significantly promoted the change in AHF, leading to the emergence of urban warming and other phenomena (Cao et al., 2019; Koralegedara et al., 2016). The energy use in buildings accounts for a large part of heat emissions, and the link between AHF and urban energy consumption is related to building scale (Zhou et al., 2012). In highly integrated regional urban groups, AH accumulation will profoundly impact (He et al., 2020). In the past two decades, China's rapid urbanization process is spawning more and more energy consumption. Yangtze River Delta region has a high degree of urban agglomeration in China, and AH forms a continuous distribution in space, resulting in a climate forcing effect that cannot be ignored. Studying the impact of building characteristics on AHF is conducive to reveal the impact of human activities on the energy balance at the surface-atmosphere interface, which is of great significance for understanding climate change in urban areas (Chen et al., 2016b; Xie et al., 2016).

Appropriate models and methods are essential for AHF estimation. The classic energy consumption inventory method is mainly based on urban energy and statistical data. It applies to large-scale regional AHF estimation and has apparent advantages in the multi-city analysis (Chen et al., 2020). The development of remote sensing technology can provide enough details to describe urban AHF. Energy consumption data is allocated to smaller spatial units using remote sensing data as indicators and processed to obtain more refined AHF results. When investigating the correlation between AHF and building characteristics, the following problems need to be resolved. On the one hand, whether the correlation between AHF and complex building characteristics applies to multi-city or urban agglomeration, and what is the change trend between them each month? On the other hand, whether there are AHF differences in different building characteristics, and how the internal differences of building characteristics affect AHF?

This study aims to analyze the correlation between different building characteristics and AHF and its change trend in typical cities of the Yangtze River Delta region. The main work carried out is: (1) The AHF results of typical cities in 2000, 2008, and 2016 were obtained based on the energy consumption inventory method and multi-source remote sensing data.

Combined with the processing of time dimension downscaling, the annual AHF was localized into monthly AHF value. (2) The spatial analysis was used to extract building density and height, and different types of building characteristics were classified. (3) The correlation between different building characteristics and AHF was analyzed, and the change characteristics of different seasons and growth regions were compared to explore the impact of building internal characteristics on AHF.

2 Study area and data

2.1 Overview of the study area

The Yangtze River Delta region's planning scope covers 27 cities in three provinces (Jiangsu, Zhejiang, and Anhui) and one municipality (Shanghai) with an area of 225,000 km^2 (Fig. 1 (a) and (b)). This region is the subtropical monsoon climate with a mean annual temperature of 16°C. The terrain is mainly plain, but in the southeast area more mountainous.

With the rapid development of the Yangtze River Delta region's economy, the regional urbanization degree is high, and the urban heat island effect has grown significantly (Du et al., 2016). Among them, the urbanization rates of Shanghai (SH), Nanjing (NJ), and Hangzhou (HZ) in 2016 were 87%, 82%, and 75%, higher than the mean level of 63% in the Yangtze River Delta region over the same period. SH, NJ, and HZ are important platforms for regional economic construction, accounting for 33.26% of the overall GDP in Yangtze River Delta (2016). Meanwhile, SH is a municipality directly under the central government and belongs to megacity according to the scale of Chinese cities; NJ, the capital of Jiangsu Province, is a megalopolis; HZ, the capital of Zhejiang Province, is a type I metropolis. It can be seen that SH, NJ, and HZ are at the core position of regional development. Selecting these cities for

AHF estimation is representative in the Yangtze River Delta region (Fig. 1 (c)).

----------[Insert Figure 1]----------

Fig. 1. The study area: (a) the location of the Yangtze River Delta region in China, (b) the composition of provinces (municipality) in the Yangtze River Delta region, (c) the location of typical cities in the Yangtze River Delta region--Shanghai, Nanjing, and Hangzhou

2.2 Data

(1) Urban building data

Using the urban classification data (http://data.ess.tsinghua.edu.cn/) in 2000, 2008, and 2016 provided by Gong et al. (2019) and the building block data in 2016 provided by Shanghai metro data technology company to extract building characteristics. The spatial resolution of the urban classification data is 30 m, representing the artificial underlying surface's thematic information. The building block data is the buildings' boundary range vector data, which records the floor numbers.

(2) Remote sensing data

In this study, the remote sensing data include nighttime light data (NTL) and normalized vegetation index (NDVI).

NTL data (https://www.ngdc.noaa.gov/eog/viirs/), from the National Oceanic and Atmospheric Administration (NOAA), including DMSP/OLS (Defense Meteorological Satellite Program's Operational Linescan System) NTL in 2000 and 2008, and Suomi-NPP/VIIRS (National Polar-orbiting Partnership Visible Infrared Imaging Radiometer Suite) NTL in 2016. DMSP/OLS NTL's spatial resolution is 30 arc seconds (about 1 km), while that of Suomi-NPP/VIIRS NTL is improved to 15 arc seconds (about 500 m). Before using the data, the projection conversion and resampling are needed to get the standardized data with a resolution of 500 m.

NDVI data is MOD13A1 product (https://ladsweb.modaps.eosdis.nasa.gov/search/), from the National Aeronautics and Space Administration (NASA). This product is a 16-day synthetic product with a spatial resolution of 500 m. Products from April to October in 2000, 2008, and 2016 were collected, and quality control was conducted based on the quality control subset to eliminate cloud impact and unreliable quality data.

(3) Statistical data

China Statistical Yearbook, *China Energy Statistical Yearbook*, and urban statistical data were used to get the Yangtze River Delta region's energy consumption and socio-economic data. Energy consumption data are collected from industry, transportation, and construction. Socio-economic data are derived from indicators such as total population, the proportion of secondary and tertiary industries. Individual missing data are allocated according to the ration of the same type indicators or estimated by a linear regression method to ensure their completeness.

(4) Meteorological data

The monthly mean air temperatures of all 27 cities in the Yangtze River Delta region in 2000, 2008, and 2016 were collected from the National Meteorological Science Data Center of China (http://data.cma.cn/). These data are the collation results of temperature observation data from multiple automatic weather stations and effectively represent the monthly temperature condition in urban areas. These data were used to reflect the Yangtze River Delta region's temperature changes and for AHF time dimension downscaling processing.

3 Methods

3.1 AHF estimation

3.1.1 Annual AHF estimation

The statistical data of energy consumption and social economy in 2000, 2008, and 2016 were collected to quantify the AHF of the urban unit in the Yangtze River Delta region. AHF can be divided into four parts according to heat flux sources: industry, construction, transportation, and human metabolism.

The heat flux of each part of AHF was calculated as follows (Chen et al., 2019; Wang et al., 2019a). (1) Industry heat flux. The total energy consumption was allocated according to the proportion of the secondary industry. Then combined with the standard coal heat, the municipal industry heat flux was obtained. (2) Construction heat flux. We obtained energy consumption indicators of wholesale, retail industry, catering, and accommodation in the energy balance sheet. The total energy consumption was allocated to obtain municipal construction heat flux based on the proportion of tertiary industry and population. (3) Transportation heat flux. The transportation heat flux was calculated by using indicators such as vehicle driving distance and fuel consumption based on civilian vehicle ownership. (4) Human metabolic heat flux. The day was divided into the active state (from 7:00 to 23:00, with the metabolic heat flux intensity of 171 W/person) and the sleep state (from 23:00 to 7:00, with the metabolic heat flux intensity of 70 W/person) (Pal et al., 2012). The municipal human metabolic heat flux was obtained combined with each city's metabolic heat flux intensity and population.

$$Q_S = Q_I + Q_C + Q_T + Q_M \quad (1)$$

Where, Q_S is the overall AHF ($W \cdot m^{-2}$), Q_I is industrial heat flux ($W \cdot m^{-2}$), Q_C is construction heat flux ($W \cdot m^{-2}$), Q_T is transportation heat flux ($W \cdot m^{-2}$), Q_M is human metabolic heat flux ($W \cdot m^{-2}$).

The municipal administrative division units' AHF results can be obtained by the above energy consumption inventory method, and the grid unit AHF will be estimated on this basis. Here, using VANUI (Vegetation adjusted NTL urban index), the index representing the intensity of human activity (Zhang et al., 2013) to establish the connection between remote sensing data and urban scale AHF.

$$VANUI = (1 - NDVI_{max}) \times NTL_{nor} \quad (2)$$

Where, $NDVI_{max}$ is the maximum of the multi-temporal NDVI. NTL_{nor} is the normalized NTL data.

The linear correlation between the mean value of AHF and VANUI in each city was fitted as the grid unit AHF estimation model. It should be noted that the deviation in the timing result needs to be corrected after the preliminary estimation. The deviation, which reflected in the underestimated aggregation of AHF, was optimized by establishing a fitting correction model for adjacent time phases (Wang et al., 2020). Finally, the AHF results of grid units with a spatial resolution of 500 m in the Yangtze River Delta region in 2000, 2008, and 2016 were obtained.

3.1.2 Time dimension downscaling of AHF

Dong et al. (2017) proposed a weighted function method based on air temperature to calculate monthly AHF. This method establishes the correlation between AH sensitivity and urban air temperature in the warm and cold seasons. It is worth noting that this correlation was based on city samples from the United States and Japan, which is not representative of the cities in this study. Therefore, we replaced all 27 cities in the Yangtze River Delta region as samples to realize the localization correction of the AHF time dimension downscaling.

The mean annual temperature of 27 cities in the Yangtze River Delta region range from is concentrated (15-19 ℃). Therefore, the original sensitivity factor function of the warm and cold seasons can be simplified, and the piecewise effect of temperature will not be considered. The monthly AHF weight function is related to air temperature as:

$$AHF_{\mathrm{m}} = AHF_{\mathrm{y}} \times \frac{\alpha_{\mathrm{m}}}{(\sum_{m=1}^{12} \alpha_{\mathrm{m}})/12} \quad (3)$$

$$\alpha_{\mathrm{m}} = |T_{\mathrm{m}} - T_{\mathrm{b}}| \times f_{\mathrm{s}} + 1 \quad (4)$$

Where, AHF_{y} is the city's mean annual AHF (W·m^{-2}), α_{m} is the monthly weight factor, T_{m} is the city's mean monthly air temperature (℃), and f_{s} is the sensitivity function. T_{b} is the air temperature (℃), corresponding to the lowest energy consumption in the year. The air temperatures of each city during the alternations of the warm and cold seasons were adopted, and T_{b} was set as 20.7°C (SH), 20.2°C (NJ), and 21.2°C (HZ).

Fig. 2 showed the sensitivity analysis results of cities in the Yangtze River Delta. Therefore, the sensitivity function can be constructed based on the cities' air temperatures in the warm and cold seasons.

$$\begin{cases} f_{\mathrm{sw}} = 0.66T_{\mathrm{yw}}^2 - 32.99T_{\mathrm{yw}} + 411.94 \\ f_{\mathrm{sc}} = -0.17T_{\mathrm{yc}}^2 + 3.00T_{\mathrm{yc}} - 8.75 \end{cases} \quad (5)$$

Where, T_{y} is the city's mean annual air temperature (℃), w and c represent the warm season and cold season, respectively.

----------[Insert Figure 2]----------

Fig. 2. (a) Warm and (b) cold season sensitivity in the Yangtze River Delta region

3.2 Coupling analysis of AHF and building characteristics

3.2.1 Building Characteristics information extraction

The grid unit's building density and height were obtained by constructing the fishing net (Guo et al., 2016). Here, the fishing net size was set according to the grid unit of AHF results (500×500 m). The range of artificial surface in 2000, 2008, and 2016 was determined based on urban classification data, and the building characteristics of each study period were obtained by integrating building block data. All AHF grids within the city scope are called whole zone AHF (WA), and the building AHF grids selected by spatial analysis are called building zone AHF (BA). For each BA, the total building area can be counted to get the building density, and the mean floor is used as the building height. To compare the characteristics of different buildings, we classified them according to building attributes. The classification limits of building density and height were 30% and 6 floors. The building characteristics were divided into four categories: high density-high height (H-H), high density-low height (H-L), low density-high height (L-H), and low density-low height (L-L).

3.2.2 Correlation computation and analysis

First, using the annual growth rate index, the growth rates of urban AHF and building characteristics were calculated. The annual growth rate eliminates the scale effect of cities and applies to the growth comparison of different cities in the same period (Fei and Zhao, 2019; Meng et al., 2020). The spatial change performance of grid AHF is similar to that of urban expansion. Using this index can better reflect the AHF annual growth in typical cities.

$$\begin{cases} AHF_{\mathrm{g}} = [({AHF_{\mathrm{end}}}/{AHF_{\mathrm{start}}})^{1/d} - 1] \times 100\% \\ BC_{\mathrm{g}} = [({BC_{\mathrm{end}}}/{BC_{\mathrm{start}}})^{1/d} - 1] \times 100\% \end{cases} \tag{6}$$

Where, AHF_{start} and AHF_{end} are the urban AHF at the beginning and end periods, BC_{start} and BC_{end} are the building characteristics at the beginning and the end periods, and d is the time span.

Next, compared the monthly AHF change characteristics of the building area.

$$\Delta AHF = \frac{\sum_{i=1}^{N} AHF_{\mathrm{Bi}}}{N} - \frac{\sum_{i=1}^{M} AHF_{\mathrm{Wi}}}{M} \tag{7}$$

Where, AHF_{Bi} is the building area AHF, N is the grid number of the building area, AHF_{Wi} is the whole city AHF, and M is the grid number of the whole city.

Then, the impact of building characteristics on AHF was evaluated. Zong et al. (2019) selected parameters ISC (impervious surface coverage) and EVI (enhanced vegetation index) to quantify the impact of urbanization on vegetation growth. Here, we replace the parameters in this evaluation method to focus on the influence relationship between AHF and building characteristics. The direct impact caused by different building characteristics leads to the urban AHF gradient difference, and the indirect impact caused by natural and human factors can also promote or aggravate the AHF changes in the process of urban development.

$$AHF_{\mathrm{c}} = (1 - BC_{\mathrm{i}}) \cdot AHF_0 + BC_{\mathrm{i}} \cdot AHF_{\mathrm{B}} \tag{8}$$

Where, BC_{i} is the building characteristics value of the grid, AHF_0 is the AHF of the grid without building impact (the grid without building characteristics). AHF_{B} is the AHF of the grid with maximum building impact (according to the BC_{i} maximum value in each city).

3.3 Study technical procedure

The technical flow of this study is as follows (Fig. 3). First, heat fluxes (industry, construction, transportation, metabolism) in the Yangtze River Delta region were calculated based on economic and energy consumption data. The VANUI index was constructed based on remote sensing data (NTL and NDVI). Building characteristics (density and height) were extracted from the urban building data. Then, the AHF estimation model was constructed to obtain the grid AHF data in 2000, 2008, and 2016. Next, combined with the meteorological data to achieve the annual AHF time dimension downscale, the monthly grid AHF results were obtained. On this basis, the coupling relationship between AHF and building characteristics was analyzed. The AHF change influence in building growth regions and the building characteristics internal difference on AHF were discussed.

----------[Insert Figure 3]----------

Fig. 3. Technical flow chart

4 Results

4.1 AHF and building characteristics of typical cities

The AHF of SH, NJ, and HZ in different periods was compared, as shown in Fig. 4. AHF estimation results showed spatial heterogeneity and have increased significantly from 2000 to 2016. The spatial distribution of AHF in SH and NJ was almost in the whole city, while HZ was accumulated in the northern region. AHF's growth in typical cities all presented the single-core expansion feature and the high AHF value aggregation located at the urban center. Correspondingly, it was also the scope where the buildings gather.

The AHF of the whole city and building area from 2000 to 2016 was analyzed. As time changes, WA and BA continued to increase, and the difference was also expanding. Although there were some differences in the AHF range of typical cities, BA values were at the same level, and the order was HZ > SH > NJ.

----------[Insert Figure 4]----------

Fig. 4. AHF spatial distribution of typical cities ((a)-(c) Shanghai, (d)-(f) Nanjing, and (g)-(i) Hangzhou) in 2000 (first column), 2008 (second column) and 2016 (third column)

The building characteristics' spatial distributions of typical cities in 2016 were drawn, as shown in Fig. 5. High density buildings were in the central urban area, which had a sizeable artificial surface; low density buildings were at the edge of the urban center, and the urbanization level was low. In SH, high height buildings were accumulated in the urban center, while in NJ and HZ, they were scattered around the urban center. According to our definition of building characteristics, in 2016, the grid cells of H-H, H-L, L-H, and L-L in SH (6403 in total) were 296, 689, 1463, and 3955; those in NJ (2259 in total) were 21, 203, 515, and 1520; those in HZ (2207 in total) were 45, 123, 784, and 1255.

Section lines were drawn along the development direction of typical cities to show the change process of building characteristics from 2000 to 2016 (Fig. 5). The results show that all typical cities have the same characteristics. Building density and height developed gently in the urban center but changed significantly in the surrounding area. Building density increased in all directions of the city. The overall trend of building height was growing, and the fluctuation was noticeable.

----------[Insert Figure 5]----------

Fig. 5. The spatial distribution of building density and height of typical cities ((a), (d)

Shanghai, (b), (e) Nanjing, and (c), (f) Hangzhou) in 2016, and changes in the direction of section lines from 2000 to 2016

We compared the annual growth rates of SH, NJ, and HZ, including AHF and building characteristics (Table 1). The mean annual growth rate of AHF in typical cities was close to 6%, and it was relatively balanced in the two growth phases. The growth rate of building characteristics in 2000-2008 was significantly higher than in 2008-2016. Besides, the growth rate of building density was always higher than that of building height. HZ had the most significant change in building characteristics, followed by SH, and the growth rate of building characteristics in NJ was relatively slow.

----------[Insert Table 1]----------

Table 1 The annual growth rate of AHF and building characteristics (%)

4.2 Monthly AHF and its change characteristic

The monthly AHF results of SH, NJ, and HZ were shown in Fig. 6. The high AHF value was in winter and reached a peak in January. In May and October, the AHF was in the lowest value for the whole year and reached another peak in July and August. The order of monthly AHF for typical cities was SH > NJ > HZ. With the year changes, the AHF of each month showed an upward trend.

----------[Insert Figure 6]----------

Fig. 6. Monthly AHF results of typical cities ((a) Shanghai, (b) Nanjing, and (c) Hangzhou) in 2000, 2008 and 2016

We compared the difference in monthly AHF between the whole city and building area (Table 2). The difference in winter months was very significant, with the mean difference in

SH, NJ, and HZ was 12.69, 16.63, and 20.36 W·m^{-2}, respectively. A city with lower WA had a more considerable difference in winter months, which may be related to the city's coverage of building grid units. The AHF difference variation in summer months was relatively stable. From May to October, the mean difference among SH, NJ, and HZ was 7.72, 11.09, and 13.20 W·m^{-2}, respectively. The aggregation effect of AHF in the building area was not significant in this period.

AHF itself is at a high value level in winter due to the intensification of various energy consumption. This significant difference characteristic shows the differentiation of AHF in the building area. Urban heat emission tends to gather in the vicinity of building area, and this difference is further intensified with the year's growth. By analyzing typical cities, it can be inferred that AHF is more significantly accumulated in the building area in winter and thus has a more profound impact on the energy balance process in the urban area of the Yangtze River Delta.

----------[Insert Table 2]----------

Table 2 Monthly AHF difference between the whole city and building area

(In the table, the color of the data is red for large difference, and green for small difference)

4.3 Correlation analysis of AHF and building characteristics

By analyzing the monthly AHF distribution of the building characteristics, an obvious stratification phenomenon could be found in Fig. 7. The AHF of building characteristic L-L was relatively lowest in each period. AHF increased with an increase in building density and height. The stratification phenomenon existed but was not significant in the summer months. The AHF of various building characteristics was accumulated in a small range in summer, and the difference increased slowly with the growth of the year. AHF difference of the building characteristics in winter months was noticeable, and different cities showed different change rules.

There was little difference in AHF of two high density building characteristics in SH in 2000. The impact of building height on the heat emissions in this period was not significant. With the urban expansion, the difference in AHF between different building heights appeared. In 2000, 2008, and 2016, the AHF difference between H-H and H-L increased significantly from 1.80 $W \cdot m^{-2}$ to 3.47 $W \cdot m^{-2}$ and then to 5.20 $W \cdot m^{-2}$. The AHF difference between L-H and L-L was maintained at 0.74-1.38 $W \cdot m^{-2}$. The two low density buildings in NJ had similar AHF distribution, and the AHF value of L-L was greater than that of L-H. Taking January as an example, the difference between them increased slowly and was 1.50 $W \cdot m^{-2}$, 1.74 $W \cdot m^{-2}$, and 2.11 $W \cdot m^{-2}$ in three periods, respectively. H-H and H-L have a significant stratification phenomenon for AHF. Also, taking January as an example, the difference between these building characteristics increased from 3.68 $W \cdot m^{-2}$ to 9.22 $W \cdot m^{-2}$ in 2000-2016. The four building characteristics in HZ showed a significant stratification phenomenon each year. With the year changes, the AHF differences between the four building characteristics were also increasing.

----------[Insert Figure 7]----------

Fig. 7. Mean AHF of different building characteristics ((a)-(c) Shanghai, (d)-(f) Nanjing, and (g)-(i) Hangzhou) in each month

The AHF impact proportion of various building characteristics in typical cities was sorted out (Fig. 8). In 2000, the proportion focused on H-H and H-L (57.92% in SH, 56.69%

in NJ, and 60.98% in HZ), the high density building characteristics were more strongly correlated with AHF. In 2008 and 2016, the proportion of H-H and H-L decreased, while the L-H and L-L proportion increased. The AHF results of typical cities in the same period were similar, reflecting the stable correlation between building characteristics and AHF in the Yangtze River Delta region. With the year changes, the proportion of the four building characteristics was balanced. In urban construction and development, buildings' morphological characteristics tend to be more and more complicated, which leads to the diversity and complexity of heat emission sources. In this way, it is more difficult to distinguish and define the difference in heat emission between different building characteristics.

----------[Insert Figure 8]----------

Fig. 8. AHF impact the proportion of different building characteristics of typical cities ((a) Shanghai, (b) Nanjing, and (c) Hangzhou)

5 Discussions

5.1 AHF change in building growth region

With the development of urbanization in the Yangtze River Delta region, both AHF and building characteristics showed an increasing trend in typical cities, but growth aggregation distributions were different in space (Fig. 9). AHF's growth aggregation feature was a significant hot spot in the central urban area, and the surrounding transition through not significant aggregation area, forming a cold spot at the edge. The growth aggregation distributions of the building showed the opposite feature. The central urban area was a cold spot, and multiple hot spot areas were formed around it. This may be related to the accelerated development of suburban towns.

Although the building characteristics have not changed significantly in the central urban area over the years, the AHF has continued to grow within this range. We believe that there are two reasons for this phenomenon. First, the city case samples selected in this study are highly developed, and the central urban area's construction tends to be saturated. The increase in human production activities in this region has led to the continuous rise of heat emissions. Second, although buildings are growing around the central urban area, high-density and large-scale building communities are still in the central area. This has a more significant impact on urban climate (Hamilton et al., 2009; Kato and Yamaguchi, 2005), reflecting higher AHF values.

----------[Insert Figure 9]----------

Fig. 9. Aggregation spatial distribution of (a)-(c) AHF, (d)-(f) building density and (g)-(i) building height (Shanghai (first column), Nanjing (second column), Hangzhou (third column))

The difference in AHF performance of building characteristics between growth and non-growth region from 2000 to 2016 was analyzed (Fig. 10). From 2000 to 2008, the difference in typical cities was different. SH's AHF in the growth region was slightly higher than that of the non-growth region, and NJ showed the opposite performance. HZ had no significant difference in growth and non-growth region. It reflects that the AHF change range in the growth and non-growth region is similar during this period. From 2008 to 2016, the differences in typical cities were similar, and the curve characteristic was consistent with the monthly AHF results. AHF of the growth region was higher than the non-growth region in most months. It shows that the AHF in the building growth region changed rapidly and increased significantly in this period. The differences in typical cities were more significant in winter months (1.94-2.23 W·m^{-2}) than in the summer months (0.59-0.94 W·m^{-2}).

----------[Insert Figure 10]----------

Fig. 10. Comparison of AHF difference between building growth and non-growth region ((a) Shanghai, (b) Nanjing, (c) Hangzhou)

5.2 Analysis of internal difference of building characteristics

In the above analysis, we integrated the density and height of buildings to compare the impact of building characteristics on AHF comprehensively. It should be noted that these two building characteristics are not equivalent to each other, which can be seen from the differentiated stratification phenomenon of typical cities in Fig. 7. To this end, we separately analyzed the contribution of building density and height to AHF (Table 3).

Building density had a significant impact on AHF, which was the main impact of building characteristics on AHF. Building height was the secondary impact source, and in NJ, it had a negative impact on AHF's performance. We believe that this result is closely related to the spatial distribution of building characteristics. The building density changed regularly from the urban center to the outside, and the distribution of building height was scattered. Analyzing the difference in each building characteristic's contribution can better understand its actual impact on heat emissions.

----------[Insert Table 3]----------

Table 3 Contribution of building density and height to AHF (%)

The variation of AHF with building density in typical months of winter and summer was analyzed and listed the top three months of typical cities in AHF ranking each season to avoid redundancy in data presentation (Fig. 11). The correlation between AHF and building density was monotonously increasing, and the greater the density, the stronger the impact on AHF. With the increase of building density, the line segments became steeper in winter, reflecting the more significant impact of building density on heat emissions. SH witnessed the fastest growth rate of AHF with building density in 2008. NJ also experienced the most rapid growth rate in 2008 and showed a significant slowdown in 2016. HZ's growth rate had been accelerating over time.

----------[Insert Figure 11]----------

Fig. 11. The correlation between AHF and building density in typical months in winter and summer, (a)-(c) Shanghai, (d)-(f) Nanjing, (g)-(i) Hangzhou

6 Conclusion

In this paper, a high spatial resolution (500m) AHF data set was established combining with energy consumption data and remote sensing products, which effectively improved the representation accuracy of AHF in the Yangtze River Delta region. Furthermore, monthly AHF was obtained by considering the time dimension downscaling processing. On this basis, combined with the building data of typical cities in the Yangtze River Delta region, the correlation and change trend of AHF and building characteristics in 2000, 2008, and 2016 were analyzed. It should be pointed out that the conclusions of this study are based on stable atmospheric conditions. Whether this study scheme is applicable to cities in other climatic zones needs more comparative verification of differential atmospheric conditions. The conclusions are as follows.

(1) From 2000 to 2016, AHF in the typical cities has increased significantly with the single core expansion feature, and high AHF value gathers at the core region. The difference in AHF between the building area and the whole city is also increasing. The building characteristics maintain the growth trend, but the growth area is accumulated around the central urban area. From 2000 to 2008, the difference between the growth and non-growth region of building in typical cities is different. From 2008 to 2016, the difference is consistent; the AHF of building growth region is higher than building non-growth region.

(2) The city's heat emissions are accumulated near the building area, and the AHF difference of building in winter is more obvious than in summer. The monthly AHF distribution of different building characteristics has a stratification phenomenon. The proportion of AHF increases with the increase of building density and height. With the development of the city, buildings' morphological characteristics tend to be complicated, leading to the diversity and complexity of heat emission sources, making it challenging to analyze the difference of AHF in different building characteristics.

(3) The influence of building density on AHF is more significant relative to building height, which is a suitable index for AHF correlation analysis. The correlation between AHF and building density is monotonically increasing, and the greater the density, the stronger the impact on AHF. The sensitivity of AHF to building density is higher in winter than in summer, which means that the impact of building density on heat emission is more significant in winter.

Acknowledgment

This work is supported by National Natural Science Foundation of China (41671339) and National Key Research and Development Program of China (2017YFB0504102). All the authors would like to thank the national and local bureau of China statistics for providing socioeconomic data and energy-consumption data. The remote sensing products provided by the National Aeronautics and Space Administration (NASA) and the National Oceanic and Atmospheric Administration (NOAA) ensure this study can proceed successfully.

References

Adelia AS, Yuan C, Liu L, Shan RQ. Effects of urban morphology on anthropogenic heat dispersion in tropical high-density residential areas. Energy and Buildings 2019; 186: 368-383.

Allen L, Lindberg F, Grimmond CSB. Global to city scale urban anthropogenic heat flux: model and variability. International Journal of Climatology 2011; 31: 1990-2005.

Boehme P, Berger M, Massier T. Estimating the building based energy consumption as an anthropogenic contribution to urban heat islands. Sustainable Cities and Society 2015; 19: 373-384.

Cao Z, Wu Z, Liu L, Chen Y, Zou Y. Assessing the relationship between anthropogenic heat release warming and building characteristics in Guangzhou: A sustainable development perspective. Science of The Total Environment 2019; 695: 133759.

Chen B, Dong L, Liu X, Shi GY, Chen L, Nakajima T, et al. Exploring the possible effect of anthropogenic heat release due to global energy consumption upon global climate: a climate model study. International Journal of Climatology 2016a; 36: 4790-4796.

Chen F, Yang X, Wu J. Simulation of the urban climate in a Chinese megacity with spatially heterogeneous anthropogenic heat data. Journal of Geophysical Research: Atmospheres 2016b; 121: 5193-5212.

Chen Q, Yang X, Ouyang Z, Zhao N, Jiang Q, Ye T, et al. Estimation of anthropogenic heat emissions in China using Cubist with points-of-interest and multisource remote sensing data. Environmental Pollution 2020; 266: 115183.

Chen S, Hu D, Wong MS, Ren H, Cao S, Yu C, et al. Characterizing spatiotemporal dynamics of anthropogenic heat fluxes: A 20-year case study in Beijing–Tianjin–Hebei region in China. Environmental Pollution 2019; 249: 923-931.

Doan VQ, Kusaka H, Nguyen TM. Roles of past, present, and future land use and anthropogenic heat release changes on urban heat island effects in Hanoi, Vietnam: Numerical experiments with a regional climate model. Sustainable Cities and Society 2019; 47: 101479.

Dong Y, Varquez ACG, Kanda M. Global anthropogenic heat flux database with high spatial resolution. Atmospheric Environment 2017; 150: 276-294.

Du H, Wang D, Wang Y, Zhao X, Qin F, Jiang H, et al. Influences of land cover types, meteorological conditions, anthropogenic heat and urban area on surface urban heat island in the Yangtze River Delta Urban Agglomeration. Science of The Total Environment 2016; 571: 461-470.

Fei W, Zhao S. Urban land expansion in China's six megacities from 1978 to 2015. Science of The Total Environment 2019; 664: 60-71.

Flanner MG. Integrating anthropogenic heat flux with global climate models. Geophysical Research Letters 2009; 36.

Gong P, Li X, Zhang W. 40-Year (1978–2017) human settlement changes in China reflected by impervious surfaces from satellite remote sensing. Science Bulletin 2019; 64: 756-763.

Guo G, Zhou X, Wu Z, Xiao R, Chen Y. Characterizing the impact of urban morphology heterogeneity on land surface temperature in Guangzhou, China. Environmental Modelling & Software 2016; 84: 427-439.

Gutiérrez E, González JE, Martilli A, Bornstein R. On the Anthropogenic Heat Fluxes Using an Air Conditioning Evaporative Cooling Parameterization for Mesoscale Urban Canopy Models. Journal of Solar Energy Engineering 2015; 137: 051005.

Hamilton IG, Davies M, Steadman P, Stone A, Ridley I, Evans S. The significance of the anthropogenic heat emissions of London's buildings: A comparison against captured shortwave solar radiation. Building and Environment 2009; 44: 807-817.

He C, Zhou L, Yao Y, Ma W, Kinney PL. Estimating spatial effects of anthropogenic heat emissions upon the urban thermal environment in an urban agglomeration area in East China. Sustainable Cities and Society 2020; 57: 102046.

Iamarino M, Beevers S, Grimmond CSB. High-resolution (space, time) anthropogenic heat emissions: London 1970–2025. International Journal of Climatology 2012; 32: 1754-1767.

Kato S, Yamaguchi Y. Analysis of urban heat-island effect using ASTER and ETM+ Data: Separation of anthropogenic heat discharge and natural heat radiation from sensible heat flux. Remote Sensing of Environment 2005; 99: 44-54.

Koralegedara SB, Lin C-Y, Sheng Y-F, Kuo C-H. Estimation of anthropogenic heat emissions in urban Taiwan and their spatial patterns. Environmental Pollution 2016; 215: 84-95.

Ma S, Pitman A, Hart M, Evans JP, Haghdadi N, MacGill I. The impact of an urban canopy and anthropogenic heat fluxes on Sydney's climate. International Journal of Climatology 2017; 37: 255-270.

Meng L, Sun Y, Zhao S. Comparing the spatial and temporal dynamics of urban expansion in Guangzhou and Shenzhen from 1975 to 2015: A case study of pioneer cities in China’s rapid urbanization. Land Use Policy 2020; 97: 104753.

Pal S, Xueref-Remy I, Ammoura L, Chazette P, Gibert F, Royer P, et al. Spatio-temporal variability of the atmospheric boundary layer depth over the Paris agglomeration: An assessment of the impact of the urban heat island intensity. Atmospheric Environment 2012; 63: 261-275.

Park C, Schade GW, Werner ND, Sailor DJ, Kim C-H. Comparative estimates of anthropogenic heat emission in relation to surface energy balance of a subtropical urban neighborhood. Atmospheric Environment 2016; 126: 182-191.

Quah AKL, Roth M. Diurnal and weekly variation of anthropogenic heat emissions in a tropical city, Singapore. Atmospheric Environment 2012; 46: 92-103.

Sailor DJ, Georgescu M, Milne JM, Hart MA. Development of a national anthropogenic heating database with an extrapolation for international cities. Atmospheric Environment 2015; 118:

7-18.
Sun R, Wang Y, Chen L. A distributed model for quantifying temporal-spatial patterns of anthropogenic heat based on energy consumption. Journal of Cleaner Production 2018; 170: 601-609.
Wang S, Hu D, Chen S, Yu C. A Partition Modeling for Anthropogenic Heat Flux Mapping in China. Remote Sensing 2019a; 11.
Wang S, Hu D, Yu C, Chen S, Di Y. Mapping China's time-series anthropogenic heat flux with inventory method and multi-source remotely sensed data. Science of The Total Environment 2020; 734: 139457.
Wang Y-C, Bian Z-F, Qin K, Zhang Y, Lei S-G. A modified building energy model coupled with urban parameterization for estimating anthropogenic heat in urban areas. Energy and Buildings 2019b; 202: 109377.
Wong MS, Yang J, Nichol J, Weng Q, Menenti M, Chan P. Modeling of Anthropogenic Heat Flux Using HJ-1B Chinese Small Satellite Image: A Study of Heterogeneous Urbanized Areas in Hong Kong. IEEE Geoscience and Remote Sensing Letters 2015; 12: 1466-1470.
Xie M, Liao J, Wang T, Zhu K, Zhuang B, Han Y, et al. Modeling of the anthropogenic heat flux and its effect on regional meteorology and air quality over the Yangtze River Delta region, China. Atmos. Chem. Phys. 2016; 16: 6071-6089.
Yang T, Gbaguidi A, Zhang W, Wang X, Wang Z, Yan P. Model-Integration of Anthropogenic Heat for Improving Air Quality Forecasts over the Beijing Megacity. Aerosol and Air Quality Research 2018; 18: 790-802.
Yuan C, Adelia AS, Mei S, He W, Li X-X, Norford L. Mitigating intensity of urban heat island by better understanding on urban morphology and anthropogenic heat dispersion. Building and Environment 2020; 176: 106876.
Zhang Q, Schaaf C, Seto KC. The Vegetation Adjusted NTL Urban Index: A new approach to reduce saturation and increase variation in nighttime luminosity. Remote Sensing of Environment 2013; 129: 32-41.
Zheng Y, Weng Q. High spatial- and temporal-resolution anthropogenic heat discharge estimation in Los Angeles County, California. Journal of Environmental Management 2018; 206: 1274-1286.
Zhong Q, Ma J, Zhao B, Wang X, Zong J, Xiao X. Assessing spatial-temporal dynamics of urban expansion, vegetation greenness and photosynthesis in megacity Shanghai, China during 2000–2016. Remote Sensing of Environment 2019; 233: 111374.
Zhou Y, Weng Q, Gurney KR, Shuai Y, Hu X. Estimation of the relationship between remotely sensed anthropogenic heat discharge and building energy use. ISPRS Journal of Photogrammetry and Remote Sensing 2012; 67: 65-72.
Ziaul S, Pal S. Anthropogenic heat flux in English Bazar town and its surroundings in West Bengal, India. Remote Sensing Applications: Society and Environment 2018; 11: 151-160.

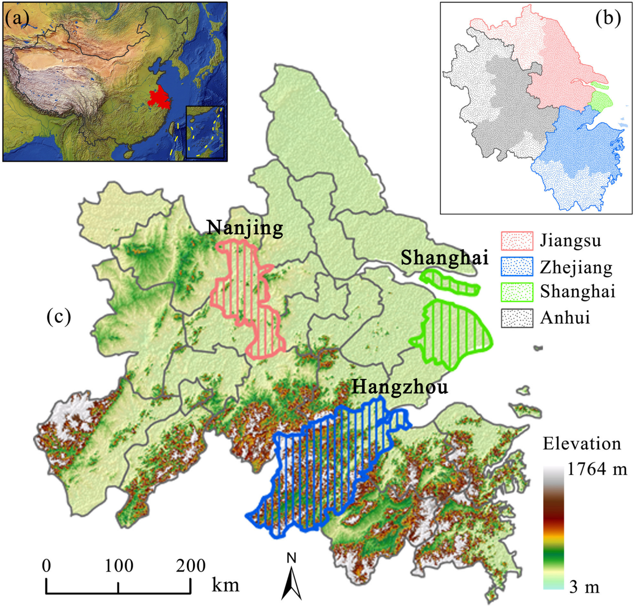

(a)
(b)
(c)
Nanjing
Shanghai
Hangzhou
Jiangsu
Zhejiang
Shanghai
Anhui
Elevation
1764 m
3 m
0
100
200
km
N

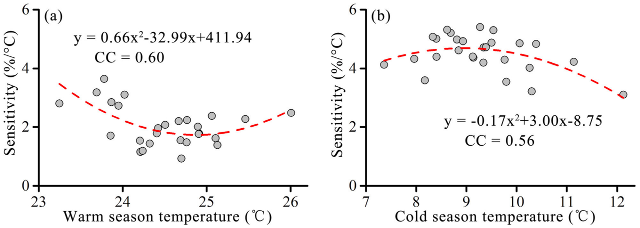

(a)
y = 0.66x²-32.99x+411.94
CC = 0.60
Sensitivity (%/°C)
Warm season temperature (℃)
(b)
y = -0.17x²+3.00x-8.75
CC = 0.56
Sensitivity (%/°C)
Cold season temperature (℃)

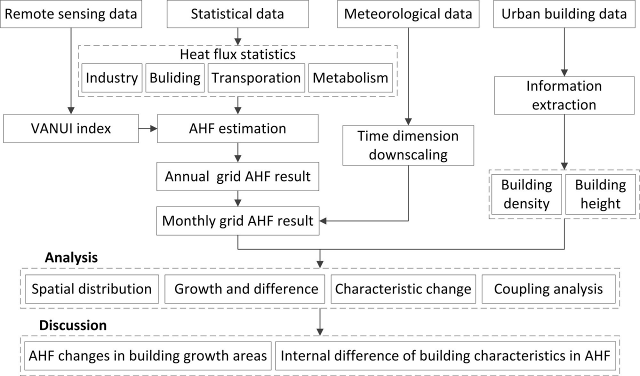

Remote sensing data
Statistical data
Meteorological data
Urban building data
Heat flux statistics
Industry
Buliding
Transporation
Metabolism
Information extraction
VANUI index
AHF estimation
Time dimension downscaling
Annual grid AHF result
Building density
Building height
Monthly grid AHF result
Analysis
Spatial distribution
Growth and difference
Characteristic change
Coupling analysis
Discussion
AHF changes in building growth areas
Internal difference of building characteristics in AHF

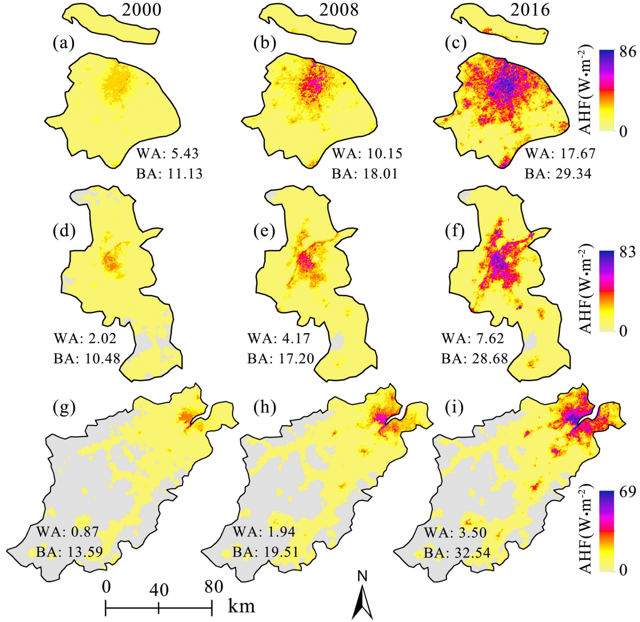
2000
2008
2016
(a)
(b)
(c)
AHF(W·m⁻²)
86
0
WA: 5.43
BA: 11.13
WA: 10.15
BA: 18.01
WA: 17.67
BA: 29.34
(d)
(e)
(f)
83
0
WA: 2.02
BA: 10.48
WA: 4.17
BA: 17.20
WA: 7.62
BA: 28.68
(g)
(h)
(i)
69
0
WA: 0.87
BA: 13.59
WA: 1.94
BA: 19.51
WA: 3.50
BA: 32.54
0
40
80
km
N

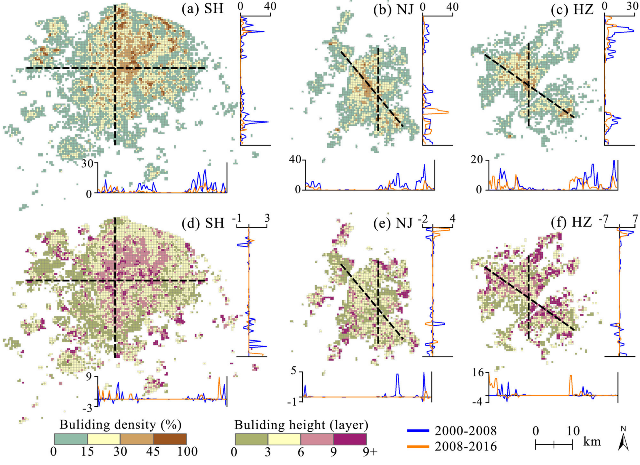
(a) SH
(b) NJ
(c) HZ
(d) SH
(e) NJ
(f) HZ
Buliding density (%)
0 15 30 45 100
Buliding height (layer)
0 3 6 9 9+
2000-2008
2008-2016
0 10 km
N

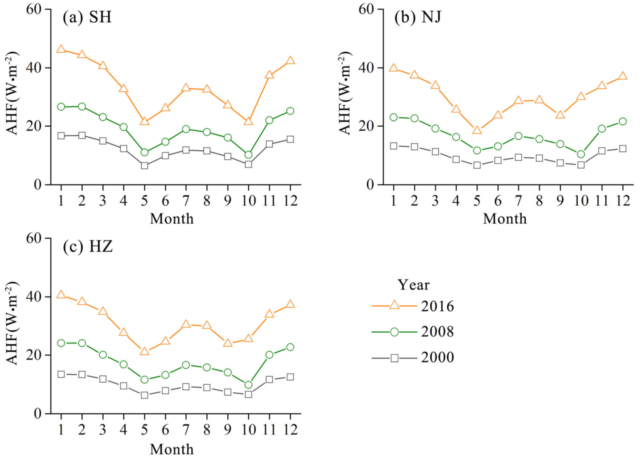

(a) SH
(b) NJ
(c) HZ
AHF(W·m⁻²)
Month
60
40
20
0
1 2 3 4 5 6 7 8 9 10 11 12
Year
2016
2008
2000

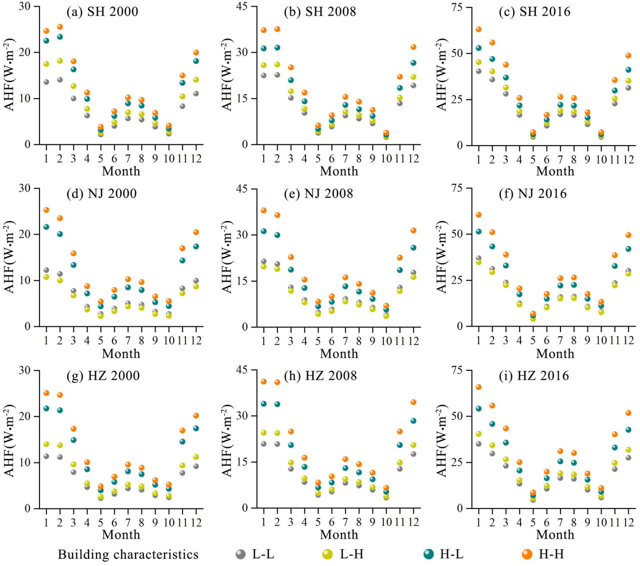

(a) SH 2000
(b) SH 2008
(c) SH 2016
(d) NJ 2000
(e) NJ 2008
(f) NJ 2016
(g) HZ 2000
(h) HZ 2008
(i) HZ 2016
AHF(W·m-2)
Month
Building characteristics
L-L
L-H
H-L
H-H

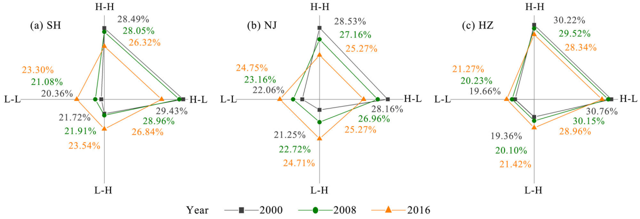

(a) SH
H-H
28.49%
28.05%
26.32%
23.30%
21.08%
20.36%
L-L
H-L
29.43%
28.96%
26.84%
21.72%
21.91%
23.54%
L-H
(b) NJ
H-H
28.53%
27.16%
25.27%
24.75%
23.16%
22.06%
L-L
H-L
28.16%
26.96%
25.27%
21.25%
22.72%
24.71%
L-H
(c) HZ
H-H
30.22%
29.52%
28.34%
21.27%
20.23%
19.66%
L-L
H-L
30.76%
30.15%
28.96%
19.36%
20.10%
21.42%
L-H
Year
2000
2008
2016

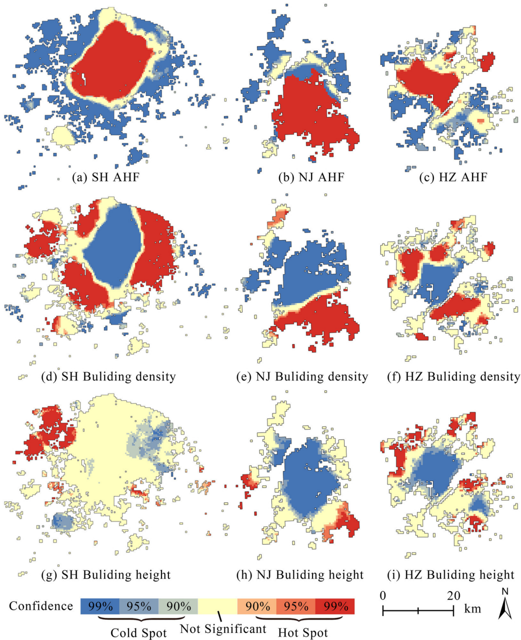
(a) SH AHF
(b) NJ AHF
(c) HZ AHF
(d) SH Buliding density
(e) NJ Buliding density
(f) HZ Buliding density
(g) SH Buliding height
(h) NJ Buliding height
(i) HZ Buliding height
Confidence
99%
95%
90%
90%
95%
99%
Cold Spot
Not Significant
Hot Spot
0
20
km
N

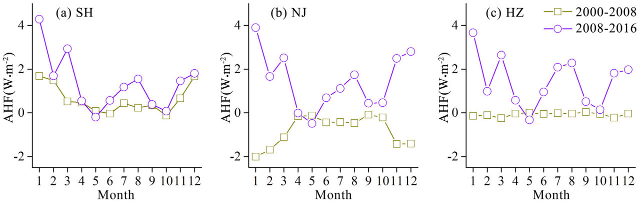

(a) SH
(b) NJ
(c) HZ
2000-2008
2008-2016
AHF(W·m-2)
Month
4
2
0
-2
1 2 3 4 5 6 7 8 9 10 11 12

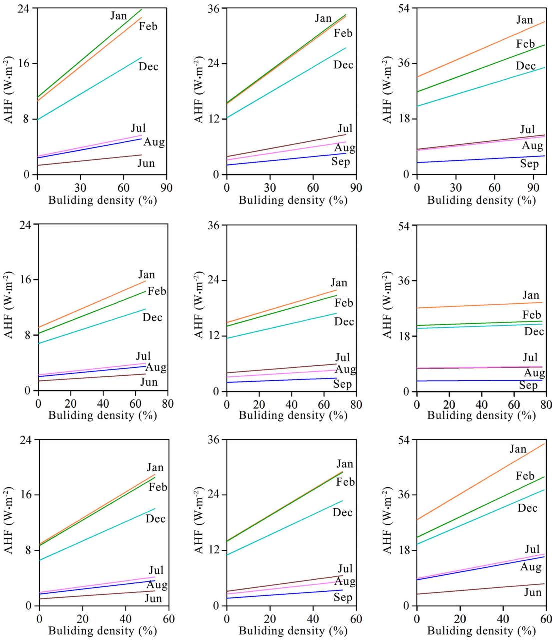
AHF (W·m⁻²)
Buliding density (%)
Jan
Feb
Dec
Jul
Aug
Jun
Sep

Table 1 The annual growth rate of AHF and building characteristics of typical cities in the Yangtze River Delta (%)

City	AHF		Building density		Building height	
	2000-2008	2008-2016	2000-2008	2008-2016	2000-2008	2008-2016
SH	5.12	6.16	5.18	2.23	2.00	1.03
NJ	6.39	6.60	4.35	2.09	1.08	0.84
HZ	6.21	6.29	5.02	3.49	2.13	1.86

Table 2 Monthly AHF difference between the whole city and building area

City	Year	Month											
		Jan	Feb	Mar	Apr	May	Jun	Jul	Aug	Sep	Oct	Nov	Dec
SH	2000	9.24	9.35	8.27	6.83	3.62	5.49	6.54	6.38	5.33	3.83	7.69	8.59
	2008	12.52	12.56	10.84	9.23	5.18	6.89	8.88	8.43	7.56	3.50	10.32	11.82
	2016	21.08	20.25	18.52	14.93	6.51	11.95	15.05	14.87	12.42	6.51	17.08	19.29
NJ	2000	10.50	10.27	8.91	6.87	5.28	6.56	7.43	7.19	5.89	5.34	9.14	9.78
	2008	17.33	17.09	14.44	12.28	8.81	9.87	12.52	11.75	10.45	7.85	14.40	16.27
	2016	29.13	27.43	24.85	18.80	8.96	17.35	21.06	21.22	17.35	14.69	24.77	27.11
HZ	2000	12.28	12.21	10.78	8.62	5.71	7.15	8.42	8.11	6.71	6.02	10.67	11.39
	2008	21.41	21.41	17.87	14.97	10.29	11.77	14.79	14.02	12.54	8.76	17.87	20.17
	2016	35.62	33.62	30.67	24.34	12.33	21.71	26.77	26.45	21.08	14.96	29.82	32.77

(In the table, the color of the data is red for large difference, and green for small difference)

Table 3 Contribution of building density and height to AHF (%)

City	Building density			Building height		
	2000	2008	2016	2000	2008	2016
SH	88.42	81.47	77.13	11.58	18.53	22.87
NJ	109.73	103.51	98.34	-9.73	-3.51	1.66
HZ	86.46	79.22	78.67	13.54	20.78	21.33

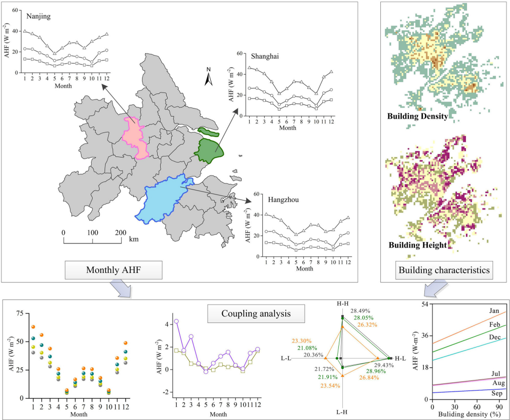

Nanjing
Shanghai
Hangzhou
AHF (W m⁻²)
Month
km
Monthly AHF
Building Density
Building Height
Building characteristics
Coupling analysis
H-H
L-L
H-L
L-H
28.49%
28.05%
26.32%
23.30%
21.08%
20.36%
21.72%
21.91%
23.54%
29.43%
28.96%
26.84%
Jan
Feb
Dec
Jul
Aug
Sep
Buliding density (%)